Journal of Power Sources 293 (2015) 498–510

Contents lists available at ScienceDirect

Journal of Power Sources

journal homepage: www.elsevier.com/locate/jpowsour

A study on effect of lithium ion battery design variables upon features of thermal-runaway using mathematical model and simulation

Chan Ho Lee*, Sang June Bae, Minyoung Jang

Battery R&D Center, Core Technology Lab, Samsung SDI Co. Ltd, 130 Samsung-ro, Yeongtong-gu, Suwon-si, Gyeonggi-do 443-803, Republic of Korea

HIGHLIGHTS

- A thermal-runaway model is developed with electrochemical and reaction model.
- A thermal-runaway model is quantitatively matched with the experimental results.
- A guideline for designing is suggested to delay onset of thermal-runaway.
- A short-circuit model is developed with short-circuit resistance and ohm's law.

ARTICLE INFO

Article history:
Received 27 January 2015
Received in revised form
28 April 2015
Accepted 22 May 2015
Available online 31 May 2015

Keywords:
Thermal-runaway
Lithium-ion battery
Exothermic reaction model
Design variable

ABSTRACT

A thermal-runaway model of lithium-ion battery is developed by devising a resistive heating that includes short circuit current and integrating it with existing electrochemical and exothermic reaction model of lithium-ion battery. With the developed model, a guideline for designing lithium-ion battery is suggested to delay onset of thermal-runaway. First and foremost, the simulation result obtained from developed mathematical model confirms that thermal-runaway is retarded when the area of heat transfer is augmented in the cells of same volume and capacity. Next, it is also demonstrated that, under the simulation condition in which the loading level of active materials is set as a design variable, if short circuit resistance is same, thermal-runaway occurs in a lithium-ion battery with high loading level whereas thermal-runaway do not occur when the loading level is low. Assuming the same area of electrical short, thermal-runaway occurs when cathode active material of 619 [J/g] is used, but thermal-runaway does not occur with the cathode active material of 429 [J/g]. If short circuit resistance is same, a cell of which the internal resistance equals 0.025 [Ω] drives itself into thermal-runaway, while cells with higher internal resistance, i.e. 0.03 [Ω], do not.

1. Introduction

Along with the growing demands from customers, recent lithium-ion batteries have more capacity and power than any other cells before. As it is widely known, safety issue comes to the fore when the capacity and power increases in lithium-ion batteries, which, in turn, calls for necessity of securing safety in design stage when developing a high-capacity, high-powered lithium-ion battery [1–8]. Safety refers to a multi-physical phenomenon in which electrochemical and exothermic reactions happen simultaneously, and thus is especially difficult to predict its quantitative data using a single mathematical model in design stage of lithium-ion battery. A phenomenon in which exothermic reaction and explosion occurs in safety tests is called thermal-runaway. Once it is initiated, the process is very rapid and dangerous due to high temperature and pressure, which interrupts quantitative measure of temperature and pressure. These difficulties in in-situ observation or measure of data in thermal-runaway calls for the development of mathematical model, and more research has been carried out on simulation concurrently with experimental research. To study thermal-runaway using simulation, building a mathematical model should precede, based on mechanism of thermal-runaway, and resistive heat generation reflecting electrochemical phenomena and chemical exothermic reaction heat must be included in the thermal-runaway model. Under these circumstances to simulate thermal-runaway, an electrochemical model developed by Newman et al. [9–21] and an exothermic reaction model based on ARC analysis by

* Corresponding author.
E-mail address: chanho75.lee@samsung.com (C.H. Lee).

http://dx.doi.org/10.1016/j.jpowsour.2015.05.095
0378-7753/

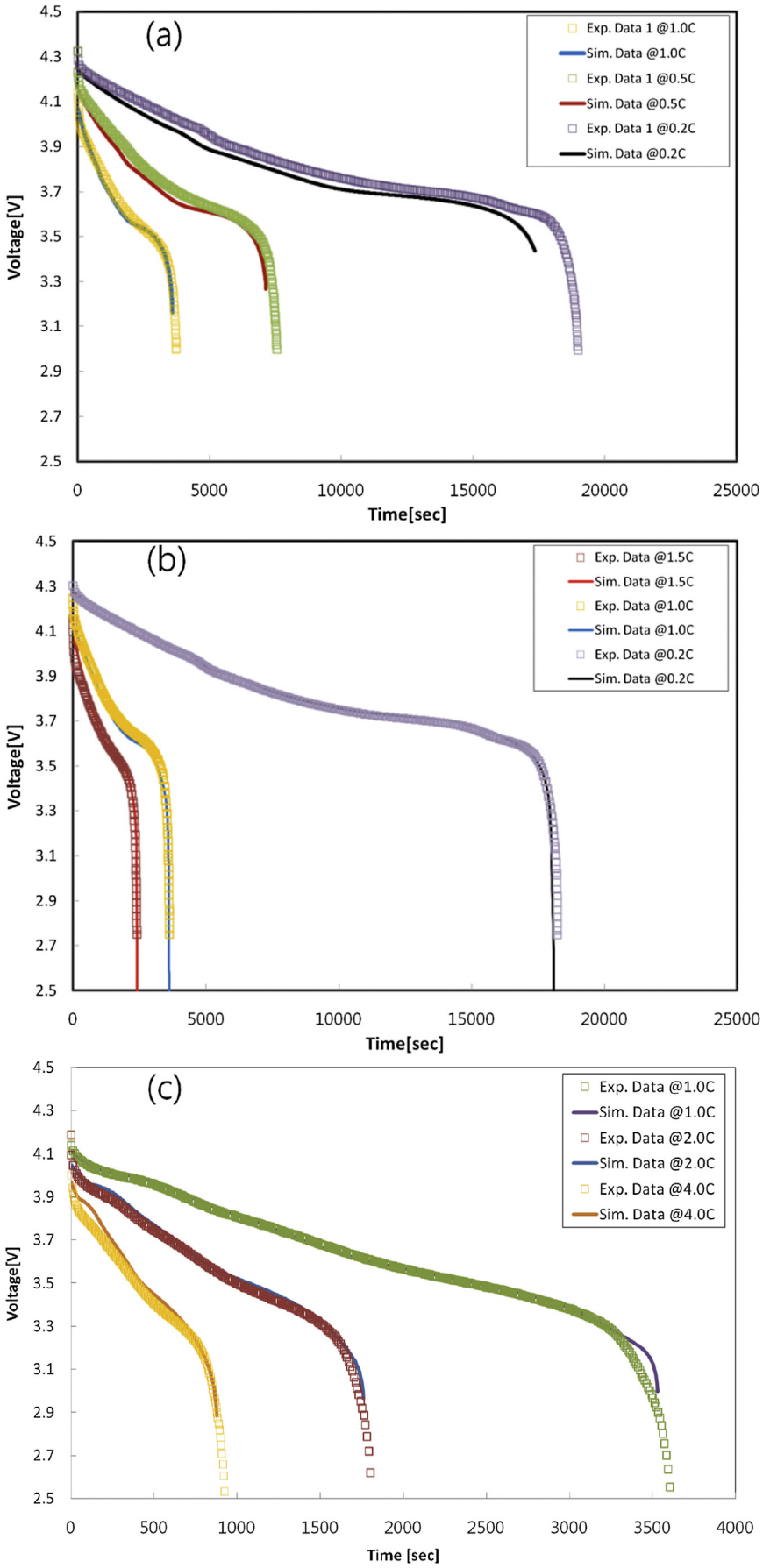

Fig. 1. Validation of electrochemical model: (a) 3.43 Ah polymer cell, (b) 2.43 Ah prismatic cell and (c) 2.5 Ah cylindrical cell.

Table 1
Cell design and electrochemical model parameter of 3.43 Ah polymer cell.

		Positive	Negative
Cell design parameter	Thickness of electrode (μm)	114	126
	Particle radius (μm)	8.25	10
	Volume fraction of solid phase	0.551	0.608
	Conductivity (S/m)	3.8	100
	Coulomic capacity (mAh/g)	167	360
	Separator thickness (μm)	15	
	Salt concentration (mol m^{-3})	1150	
	cell cross section area (m^2)	0.118864	
Model adjusting parameter	Diffusion coefficient in solid (m^2 s^{-1})	1.00E-13	3.90E-14
	Reaction rate coefficient (m/s)	2.00E-11	1.60E-12
	Salt diffusion coefficient (m^2 s^{-1})	1.87E-11	

Table 2
Cell design and electrochemical model parameter of 2.43 Ah prismatic cell.

		Positive	Negative
Cell design parameter	Thickness of electrode (μm)	129	140
	Particle radius (μm)	8.25	9
	Volume fraction of solid phase	0.466	0.533
	Conductivity (S/m)	3.8	100
	Coulomic capacity (mAh/g)	165	365
	Separator thickness (μm)	14	
	Salt concentration (mol m^{-3})	1150	
	Cell cross section area (m^2)	0.068482	
Model adjusting parameter	Diffusion coefficient in solid (m^2 s^{-1})	9.00E-13	3.00E-13
	Reaction rate coefficient (m/s)	4.00E-11	3.20E-12
	Salt diffusion coefficient (m^2 s^{-1})	1.99E-11	

Table 3
Cell design and electrochemical model parameter of 2.5 Ah cylindrical cell.

		Positive	Negative
Cell design parameter	Thickness of electrode (μm)	92	101
	Particle radius (μm)	6	7.5
	Volume fraction of solid phase	0.431	0.518
	Conductivity (S/m)	3.8	100
	Coulomic capacity (mAh/g)	185	390
	Separator thickness (μm)	18	
	Salt concentration (mol m^{-3})	1150	
	Cell cross section area (m^2)	0.10335	
Model adjusting parameter	Diffusion coefficient in solid (m^2 s^{-1})	5.80E-13	5.10E-13
	Reaction rate coefficient (m/s)	5.00E-11	5.00E-11
	Salt diffusion coefficient (m^2 s^{-1})	5.90E-11	

Table 4
Heat generation and onset point of reactions – 3.43 Ah polymer cell.

		O_2 generation			
		On set point (°C)	1st peak maximum (°C)	2nd peak maximum (°C)	Calorie (J/g)
(+)	side	205	235	288	626
	Core	196	223	277	611
	AVG	**201**	**229**	**283**	**618**

		SEI decomposition		Intercalated Li ion – binder reaction	
		On set point (°C)	Calorie (J/g)	On set point (°C)	Calorie (J/g)
(–)	Side	108	39	251	268
	Core	151	24	255	452
	AVG	**130**	**31**	**253**	**360**

Dahn et al. [22–25], are utilized up to nowadays for electrical short circuit and exothermic reaction feature, respectively, considering their efficiency and accuracy. However, preceding research of simulation targeting thermal-runaway focuses only on a specific safety test while a lithium-ion battery must pass a variety kind of tests including thermal exposure, over charge, electrical short, nail penetration, impact, crush and drop, which seriously restricts the application of its result [26–30]. Kim et al. [26] performed simulation of thermal exposure test, whereas Chen et al. [28] focused on nail penetration test. Moreover, a guideline for designing commercial cells to delay or retard onset of thermal-runaway by verifying the effect of design variables has not been suggested from any other research yet. Reflecting the circumstance, a methodology suggested in this paper combining an additional short circuit model

Table 5
Heat generation and onset point of reactions – 2.43 Ah prismatic cell.

		O_2 generation			
		On set point (°C)	1st peak maximum (°C)	2nd peak maximum (°C)	Calorie (J/g)
(+)	side	204	233	285	752
	Core	206	249	292	847
	AVG	**205**	**241**	**289**	**799**

		SEI decomposition		Intercalated Li ion – binder reaction	
		On set point (°C)	Calorie (J/g)	On set point (°C)	Calorie (J/g)
(−)	Side	151	64	228	264
	Core	152	78	223	775
	AVG	**152**	**71**	**226**	**520**

Table 6
Heat generation and onset point of reactions – 2.5 Ah cylindrical cell.

		O_2 generation			
		On set point (°C)	1st peak maximum (°C)	2nd peak maximum (°C)	Calorie (J/g)
(+)	side	181	209	264	274
	Core	177	206	261	252
	AVG	**179**	**208**	**263**	**263**

		SEI decomposition 1		SEI decomposition 2		Intercalated Li ion – binder reaction	
		On set point (°C)	Calorie (J/g)	On set point (°C)	Calorie (J/g)	On set point (°C)	Calorie (J/g)
(−)	Side	69	78	123	31	183	643
	Core	73	22	122	93	227	571
	AVG	**71**	**50**	**123**	**62**	**205**	**607**

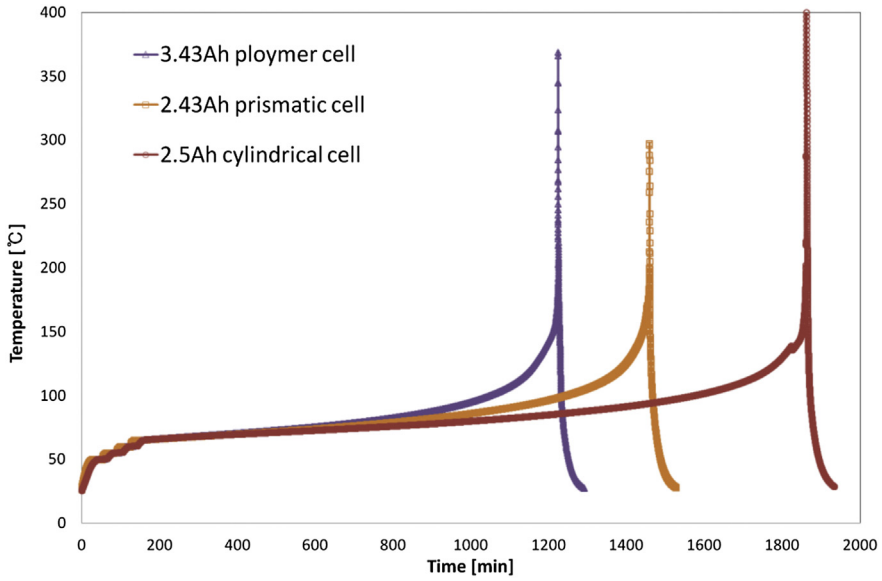

Fig. 2. Raw data of ARC measurement: temperature vs. time of 3.43 A h polymer cell, 2.43 Ah prismatic cell & 2.5 Ah cylindrical cell.

with preexisting electrochemical and exothermic reaction model completes the thermal-runaway model for a lithium-ion battery. The developed model articulates cell design concept to delay onset of thermal-runaway and analyzes clout of each design variable, making it easier to predict cell behavior. To simulate the resistance heating and thermal runaway, Newman's electrochemical model and Dahn's exothermic reaction model were applied to our study. Several researches were studied active material's surface coatings after above mentioned model had developed. And some of research was applied to commercial LIB. However, surface coatings of active material were not applied to thermal runaway model in our study that further research will be carried out to obtain thermal runaway model with surface coating of active materials.

2. Mathematical model for thermal-runaway

2.1. Electrochemical and short circuit model

In this research, Newman's mathematical model is applied to analyze electrochemical nature of a lithium-ion battery, of which primary physical phenomena are listed as follows [9,10]:

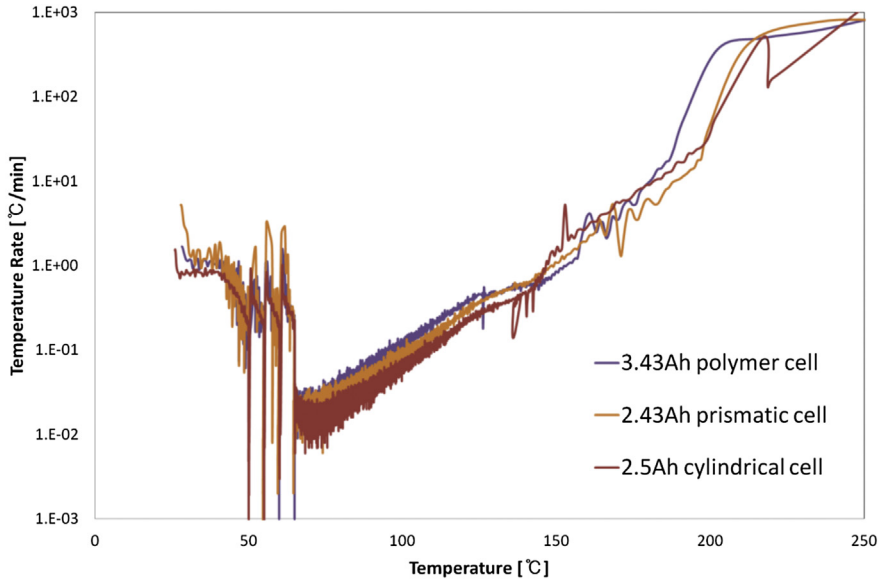

Fig. 3. Raw data of ARC measurement: temperature rate vs. temperature of 3.43 Ah polymer cell, 2.43 Ah prismatic cell & 2.5 Ah cylindrical cell.

(1) Transport of Lithium to/from surface of a particle
(2) Electrochemical oxidation/reduction of Li/Li^+ at the surface of particle
(3) Transport of Li^+ in liquid phase from anode to cathode region
(4) Potential distribution in solid and liquid phases
(5) Temperature effects on each of these process

Transport of lithium ions in electrolyte is modeled with porous electrode theory. Because porous electrode theory treats the electrode as a superposition of solid and liquid phases, the electrochemical reaction enters the equation as a homogenous term rather than as a boundary condition as follows.

$$\varepsilon_i \frac{\partial C}{\partial t} = \frac{\partial}{\partial x}\left(\varepsilon_i D_i \frac{\partial C}{\partial x}\right) + a j_{n,i}\left(1 - t^+\right) \tag{1}$$

where, C is concentration of salt in electrolyte, ε_i is porosity of region i, D_i is diffusion coefficient of Li^+ in region i, $j_{n,i}$ is particle surface flux in region i, a is specific interfacial area and t^+ is transference number.

The total current density is conserved as follows

$$I_{total} = i_1 + i_2 \tag{2}$$

where, i_1 is solid phase current density and i_2 is electrolyte phase current density. The current flowing in the solid phase is governed by Ohm's law as follows.

$$i_1 = -\sigma_i \frac{\partial \varphi_1}{\partial x} \tag{3}$$

where, ϕ_1 is electric potential of solid phase. The variation of potential in the electrolyte is governed by modified Ohm's law as follows.

$$i_2 = -\kappa_i \frac{\partial \varphi_2}{\partial x} + \frac{2\kappa_i RT}{F}\left(1 - t^+\right)\frac{1}{C}\frac{\partial C}{\partial x} \tag{4}$$

where, σ_i is solid phase conductivity, κ_i is liquid phase conductivity, ϕ_2 is electric potential of electrolyte phase, R is gas constant, T is temperature and F is faraday's constant.

The active electrode material is assumed to be made up of spherical particles of radius R_s with diffusion being the mechanism of transport of the lithium into the particle. Therefore, transport of lithium in active materials is governed by diffusion equation as follows.

$$\frac{\partial c_s}{\partial t} = \frac{1}{r^2}\frac{\partial}{\partial r}\left(D_s r^2 \frac{\partial c_s}{\partial r}\right) \tag{5}$$

where, c_s is concentration of lithium in electrode and D_s is solid phase lithium diffusivity. From symmetry, the first boundary condition is as follows.

$$\frac{\partial c_s(0,t)}{\partial r} = 0 \tag{6}$$

The second boundary condition is provided by a relationship between the pore-wall flux across the interface and the rate of diffusion of lithium ions into the surface of the active material as follows.

$$-D_s \frac{\partial c_s(R_s,t)}{\partial r} = a j_n \tag{7}$$

where, R_s is radius of electrode particle and the Butler–Volmer rate equation is used for surface reaction kinetics, j_n, as follows.

$$j_n = \frac{i_{0,k}}{F}\left[\exp\left(\frac{\alpha_{a,k}F}{RT}\eta_{s,k}\right) - \exp\left(-\frac{\alpha_{c,k}F}{RT}\eta_{s,k}\right)\right] \tag{8}$$

where, α is symmetric factor, $i_{0,k}$ is exchange current density and $\eta_{s,k}$ is over potential which are defined as follows.

$$i_{0,k} = F\left(k_{a,k}\right)^{\alpha_{c,k}}\left(k_{c,k}\right)^{\alpha_{a,k}}\left(C_{\mathrm{smax},k} - C_{s,k}\right)^{\alpha_{c,k}}\left(C_{s,k}\right)^{\alpha_{a,k}} \tag{9}$$

$$\eta_{s,k} = \varphi_1 - \varphi_2 - U_k \tag{10}$$

where, U_k is open circuit potential and function of x_k that is state of charge in active materials.

If constant current is used boundary condition of total current density, I_{total} then the galvanostatic charge and discharge simulation have been executed. But Equation (11) is used boundary condition of total current density, I_{total} then external short-circuit simulation have been executed.

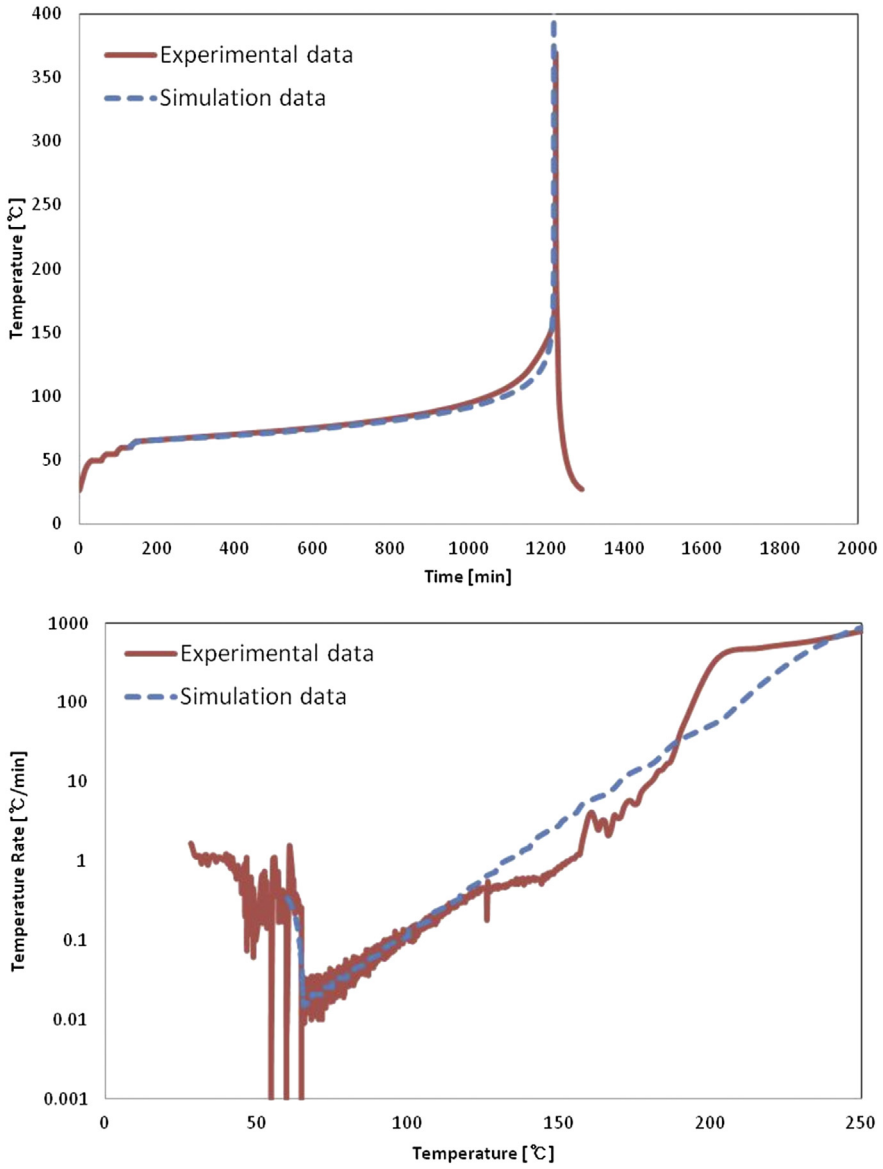

Fig. 4. Arc simulation data validation: 3.43 Ah polymer cell.

$$I_{total} = \frac{\varphi_1}{R_{external\ short}} \tag{11}$$

where, $R_{external\ short}$ is short-circuit resistance. The conservation of energy in jelly-roll of the lithium-ion batteries as follows.

$$\rho C_p \frac{dT}{dt} = \lambda \frac{\partial^2 T}{\partial x^2} + Q_{rxn} + Q_{rev} + Q_{ohm} \tag{12}$$

where ρ is density, C_p is heat capacity, λ is thermal conductivity and heat sources Q are given by

$$Q_{rxn} = FaJ(\varphi_1 - \varphi_2 - U) \tag{13}$$

$$Q_{rev} = FaJT \frac{\partial U}{\partial T} \tag{14}$$

$$Q_{ohm} = \sigma_{eff} \left(\frac{\partial \varphi_1}{\partial x}\right)^2 + \kappa_{eff} \left(\frac{\partial \varphi_2}{\partial x}\right)^2 + \frac{2\kappa_{eff} RT}{F} \left(1 - t_+^0\right) \frac{1}{c} \frac{\partial c}{\partial x} \frac{\partial \varphi_2}{\partial x} \tag{15}$$

The additional heat source in short-circuit region of the lithium-ion batteries as follows.

$$Q_{short-circuit} = a \cdot I^2 \cdot R_{external\ short} \tag{16}$$

2.2. Exothermic reaction model and energy balance

Dahn's mathematical model formulated through ARC analysis is used to explain exothermic reaction arising in safety test [23,24]. Since Dahn et al. confirmed that the decomposition of electrolyte proceeds in such temperature over 200 °C, in the model, exothermic reactions occurring below 200 °C are categorized in 3 sections: decomposition of SEI layers, Li reaction with electrolyte in anode, and cathode reaction with electrolyte [22]. Decomposition of SEI layer is the first reaction in ARC experiment because the

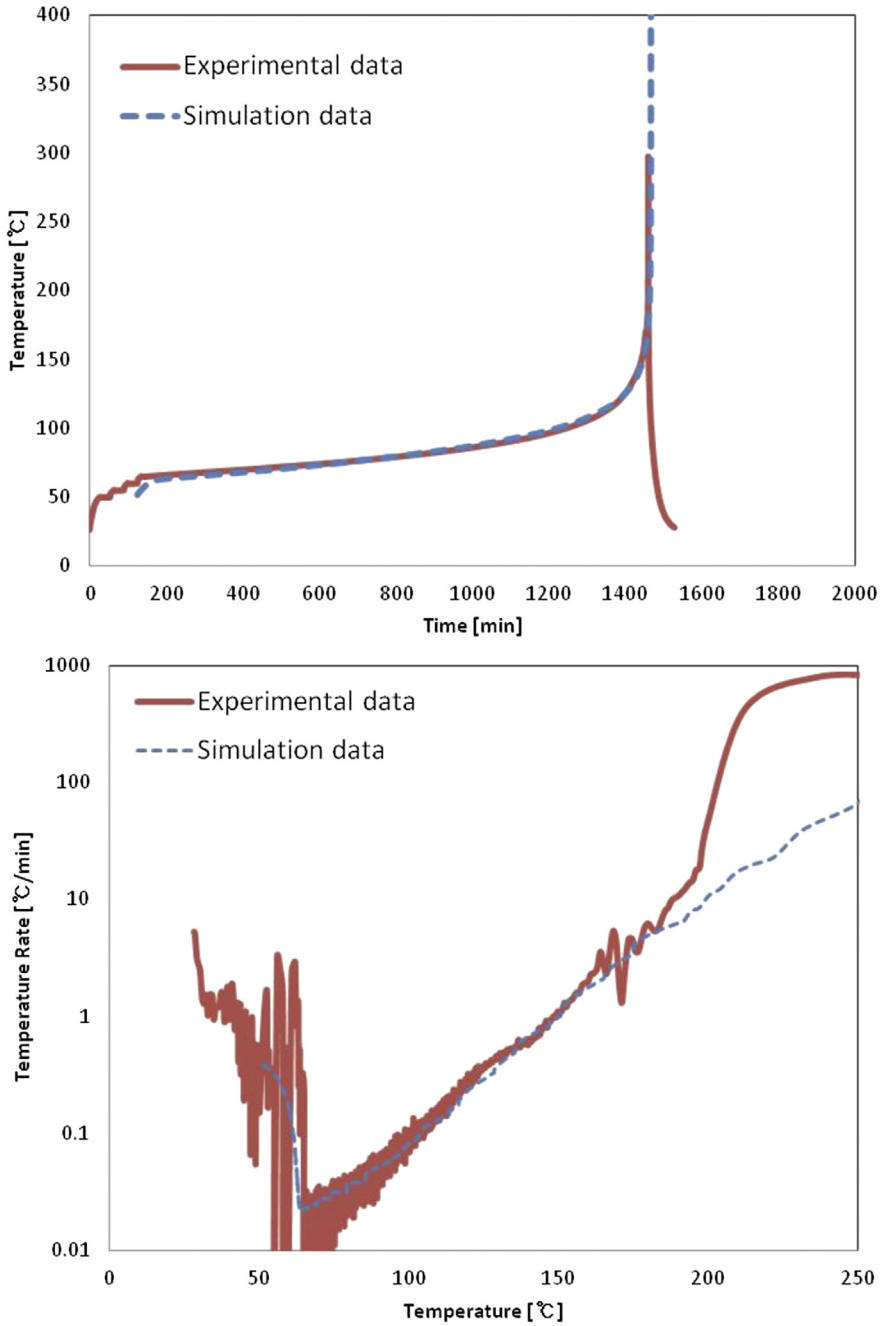

Fig. 5. Arc simulation data validation: 2.43 Ah prismatic cell.

reaction onset time is lowest among the three exothermic reactions. Therefore, SEI decomposition is very important because the onset temperature of exothermic reaction can be determined when comparing thermal safety about different kinds of LIB. Because the rate of each reaction differs from one to another, respective Arrhenius-type reaction equation applies as below.

Decomposition of SEI layer:

$$\frac{\partial x_f}{\partial t} = -A_1 \cdot \exp\left(\frac{-E_1}{k_B \cdot T}\right) \cdot x_f \tag{17}$$

where, x_f is amount of meta-stable SEI, A is frequency factor, E is activation energy and k_B is Boltzmann's constant.

Li reaction with electrolyte in anode:

$$\frac{\partial x_i}{\partial t} = -A_2 \cdot \exp\left(\frac{-E_2}{k_B \cdot T}\right) \cdot x_i \cdot \exp\left(-\frac{z}{z_0}\right) \tag{18}$$

$$\frac{\partial z}{\partial t} = A_2 \cdot \exp\left(\frac{-E_2}{k_B \cdot T}\right) \cdot x_i \cdot \exp\left(-\frac{z}{z_0}\right) \tag{19}$$

where, x_i is amount of intercalated lithium and z is amount of lithium in the SEI per unit surface area.

Cathode reaction with electrolyte:

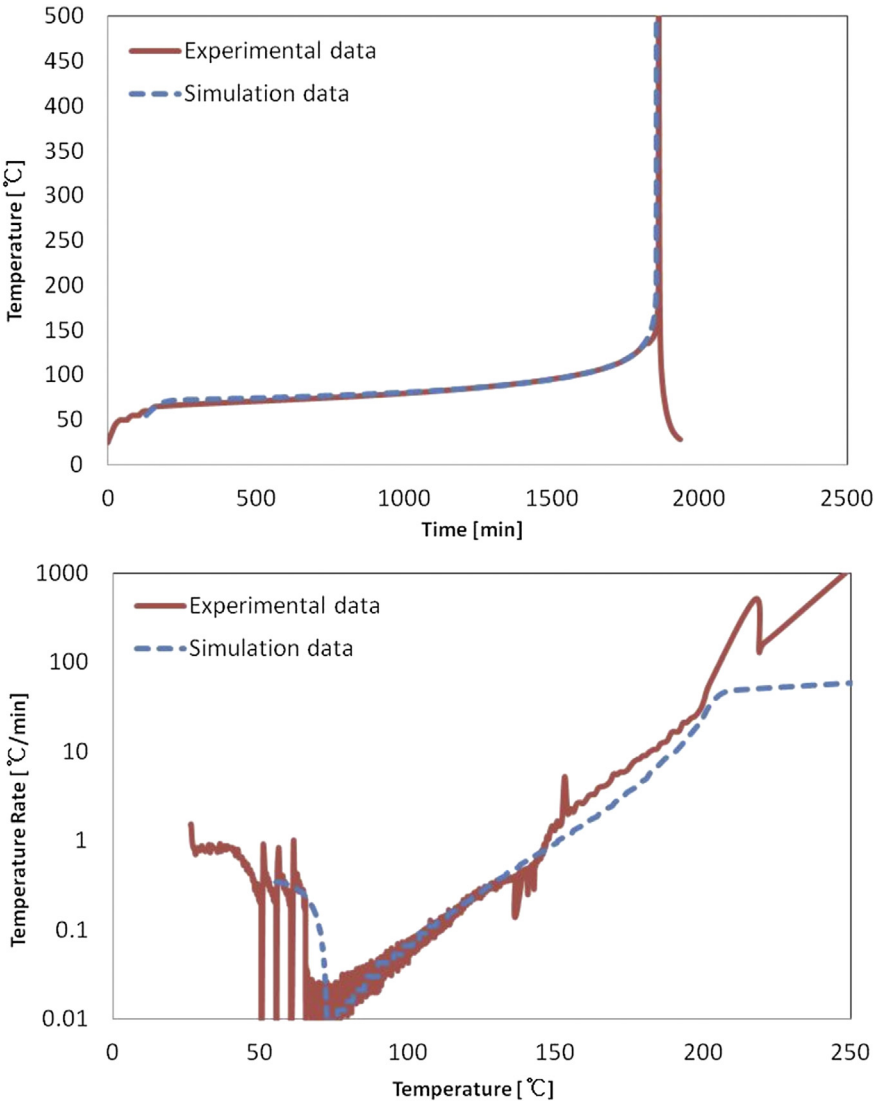

Fig. 6. Arc simulation data validation: 2.5 Ah cylindrical cell.

$$\frac{\partial u}{\partial t} = A_3 \cdot \exp\left(\frac{-E_3}{k_B \cdot T}\right) \cdot (1-u) \cdot (\beta + u) \tag{20}$$

where, u is degree of conversion and β is parameter of autocatalysis.

Reference explains physical interpretation of each equation above. Further, under adiabatic condition, the energy balance equation below elucidates temperature change from exothermic reaction [22–24].

Table 7
ARC simulation model parameter of 3.43 Ah polymer cell.

Params	G1LH
h_1_C [J/g]	31
h_2_C [J/g]	360
h_3_C [J/g]	618
A1 [1/min]	4.20.E+06
E1 [eV]	0.63
x_f0 [−]	0.15
A2 [1/min]	9.00.E+13
E2 [eV]	1.32
x_i0 [−]	0.75
k_B	0.0000862
z_0 [−]	0.033
A3 [1/min]	1.67.E+07
E3 [eV]	0.88
Beta [−]	0.03
T_0 [°C]	60

Table 8
ARC simulation model parameter of 2.43 Ah prismatic cell.

Params	PJ7A
h_1_C [J/g]	71
h_2_C [J/g]	519
h_3_C [J/g]	799
A1 [1/min]	2.85.E+05
E1 [eV]	0.56
x_f0 [−]	0.15
A2 [1/min]	4.55.E+03
E2 [eV]	0.62
x_i0 [−]	0.75
k_B	0.0000862
z_0 [−]	0.033
A3 [1/min]	6.50.E+04
E3 [eV]	0.73
Beta [−]	0.08
T_0 [°C]	51

Table 9
ARC simulation model parameter of 2.5 Ah cylindrical cell.

Params	25R
h_1_C [J/g]	112
h_2_C [J/g]	607
h_3_C [J/g]	263
A1 [1/min]	4.00.E + 04
E1 [eV]	0.53
x_f0 [−]	0.15
A2 [1/min]	3.80.E + 14
E2 [eV]	1.42
x_i0 [−]	0.75
k_B	0.0000862
z_0 [−]	0.033
A3 [1/min]	2.20.E + 15
E3 [eV]	1.65
Beta [−]	0.08
T_0 [°C]	55

$$\frac{\partial T}{\partial t} = \frac{h_1}{C_p} A_1 \cdot x_f \cdot \exp\left(\frac{-E_1}{k_B \cdot T}\right) + \frac{h_2}{C_p} A_2 \cdot x_i \cdot \exp\left(-\frac{z}{z_0}\right) \cdot \exp\left(\frac{-E_2}{k_B \cdot T}\right) + \frac{h_3}{C_p} A_3 \cdot (1-u) \cdot (\beta + u) \cdot \exp\left(\frac{-E_3}{k_B \cdot T}\right) \quad (21)$$

where, h is specific energy of each exothermic reaction.

3. Thermal-runaway model parameter characterization

3.1. Electrochemical model parameter validation

In this chapter, cell characterization of electrochemical model is carried out to quantify electrical short circuit feature which initiates thermal-runaway in safety test, for 3 different kinds of cells, namely, cylindrical, prismatic, and polymer cell. Each cell consists of different cathode active material, possessing its own capacity as well; NCA is used in a 2.5 Ah cylindrical cell and LCO is used in both 2.43 Ah prismatic cell and 3.43 Ah polymer cell. Graphite features as anode active material for the all three cells. To determine electrochemical model parameter, the followings are considered: OCV data of active materials, ionic conductivity of electrolyte, and design variables of electrodes including diameter of active materials,

Table 10
Relationship of heat transfer area and thermal-runaway − simulation case.

	Volume [mm^3]	Surface area [mm^2]	Surface/volume ratio
Case 1	15,850	15,720	0.992
Case 2		19,030	1.200
Case 3		24,180	1.526
Case 4		33,190	2.094

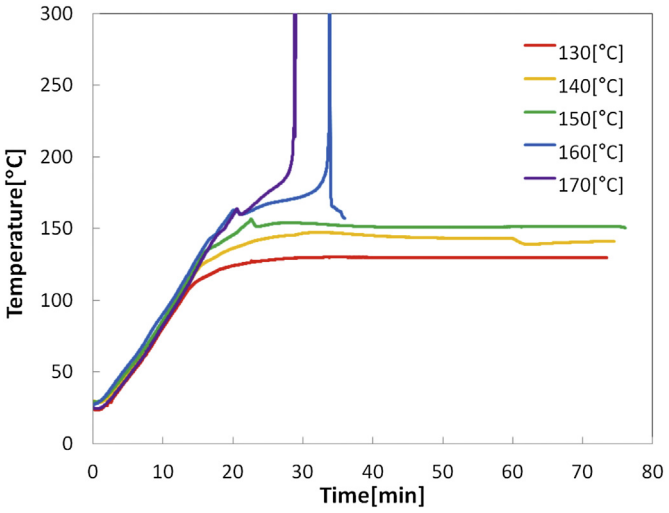

Fig. 8. Oven test experimental results under external temperature 130–170 [°C].

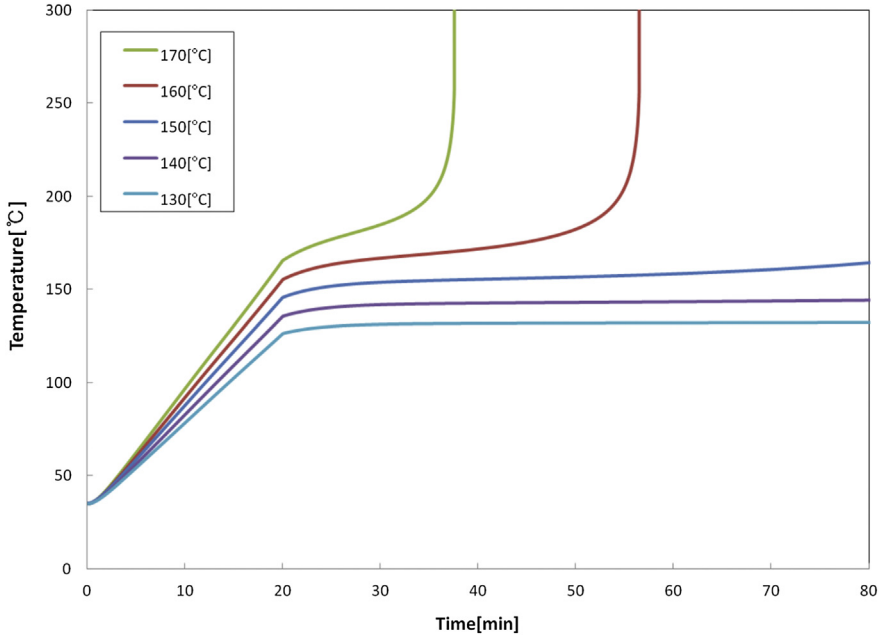

Fig. 7. Oven test simulation results under external temperature 130–170 [°C].

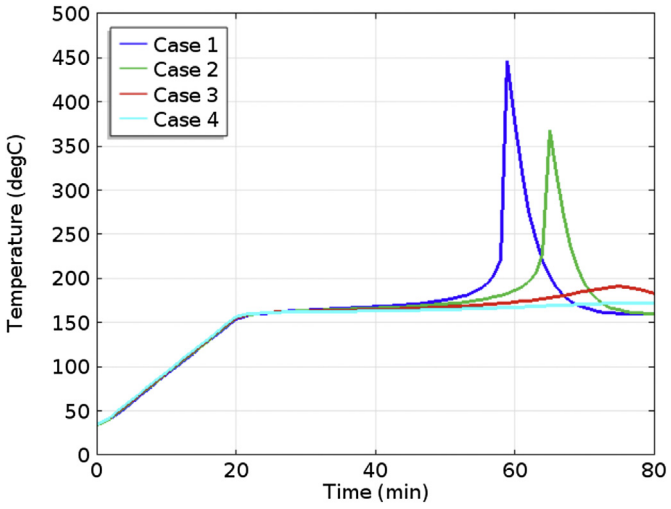

Fig. 9. Relationship of heat transfer area and thermal-runaway.

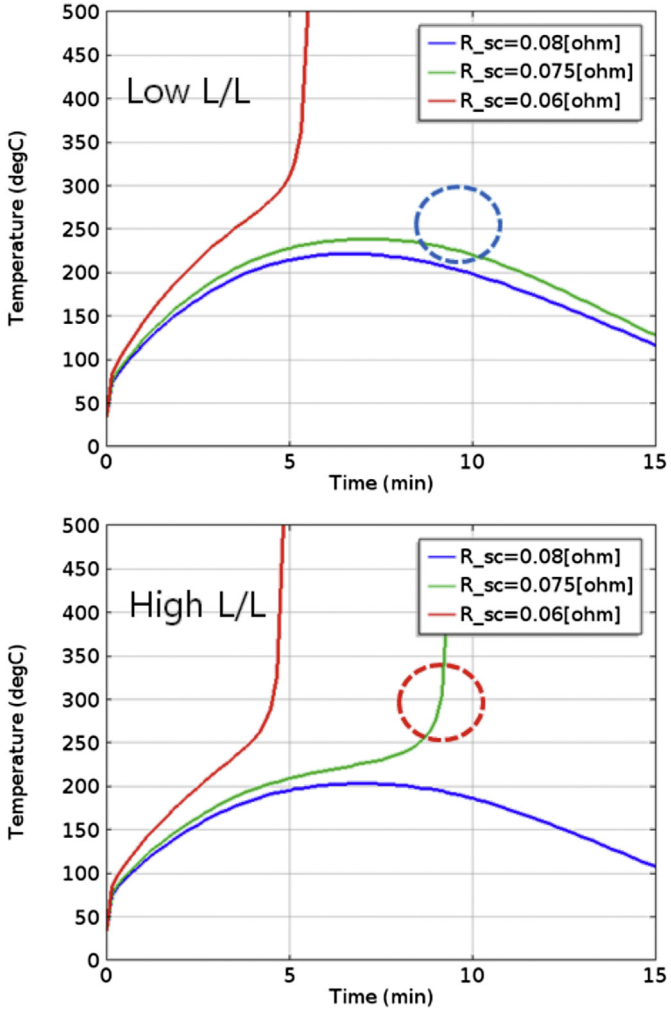

Fig. 10. Relationship of loading level of electrode and thermal-runaway.

porosity, area, thickness and salt concentration of electrolyte. Other parameters of electrochemical model not discussed above are shown in Fig. 1, which are obtained from comparing

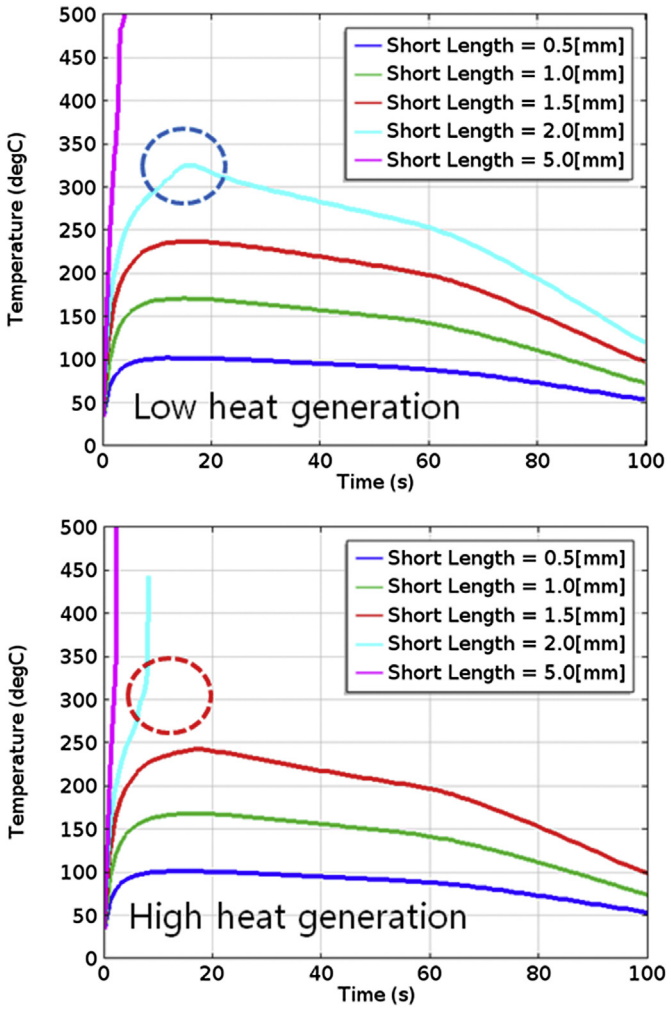

Fig. 11. Relationship of heat generation of active material and thermal-runaway.

the simulation result with galvanostatic discharge curve of a commercialized cell. Basic cell design information and electrochemical model parameters which are used in the simulation result of Fig. 1 are shown in Tables 1–3.

3.2. Exothermic reaction model parameter characterization

DSC analysis and ARC measurement are required for the three cells mentioned above to quantify heat generation and exothermic reaction rate during thermal-runaway process. For DSC analysis, Q1000 of TA Instrument is utilized. The samples for heat generation analysis are made in such a way that three different kinds of cells cited in Tables 1–3 are disassembled after being fully charged, and then each end of both electrodes is sealed hermetically while punched in a circle with diameter of 3 mm. Heat generation is measured based on the weight of active material in sample excluding metal substance from the sample. In DSC analysis, temperature is tracked from 40[°C] to 400[°C], while monotonically increased at the rate of 10[°C/min] under dry air condition. Tables 4–6 summarize heat generation and onset point of reaction of each sample. For ARC measurement, on the other hand, ES ARC of THT co. ltd. is utilized. The analysis of exothermic reaction rate employs the following conditions for measurement: initial temperature of 50[°C], terminal temperature of 350 [°C], temperature increment of 5 [°C], temperature

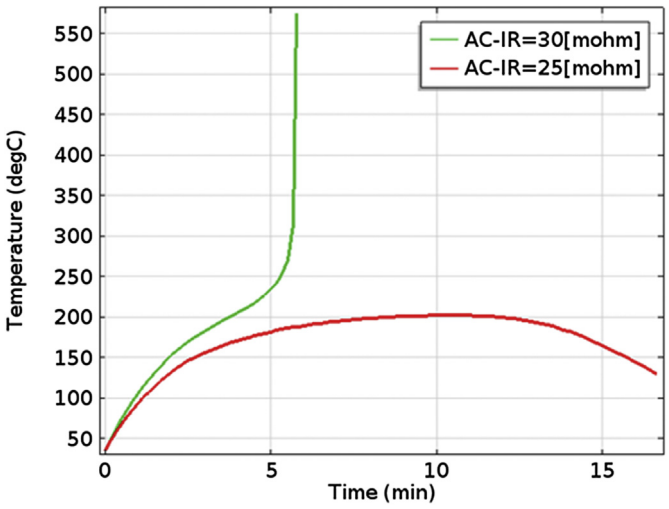

Fig. 12. Relationship of internal resistance (AC-IR) and thermal-runaway.

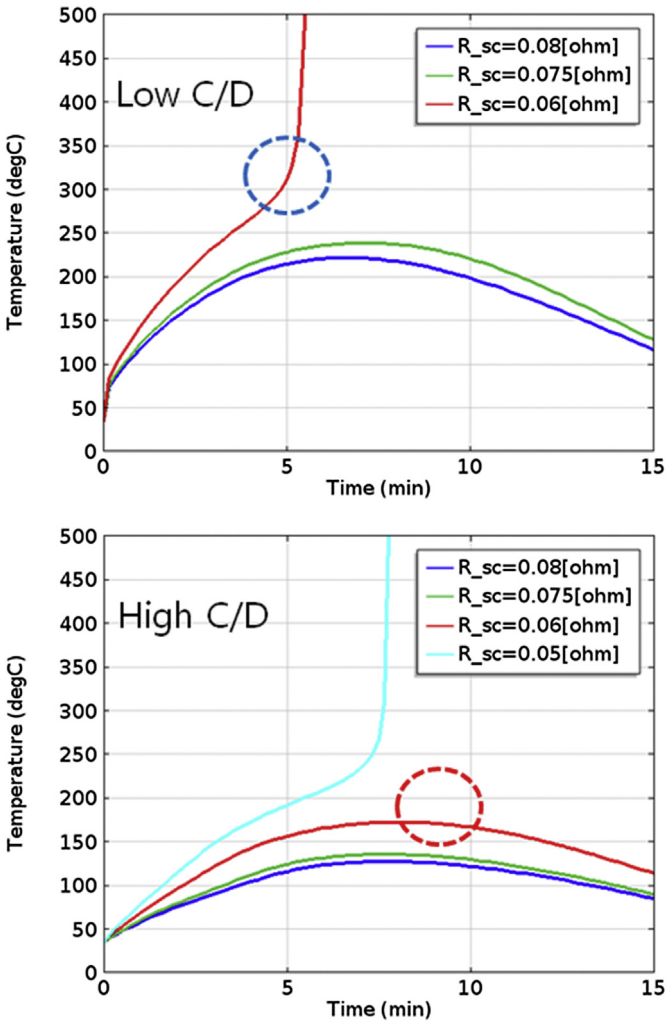

Fig. 13. Relationship of current density and thermal-runaway.

change sensitivity of 0.02 [°C/min], and waiting time for seeking self heat generation of 15 [min]. Fig. 2–3 display the temperature and temperature slope by ARC measurement. To define exothermic reaction rate coefficient such as activation energy E_1 and frequency factor A_1, the slope and y-intercept of ln(dT/dt) vs. $1/T°(K^{-1})$ graph proposed by Dahn et al. are used. Activation energy E_2, E_3 and frequency factor A_2, A_3 of the other reactions, are resolved by comparing the simulation result with the experiment result plotting temperature vs. time and temperature slope vs. temperature. Those reaction rate coefficients are arranged in Fig. 4–6 and Tables 7–9. The reason of noises in temperature rate plot by temperature as follows. The noise was generated during differentiation for temperature change by time in raw data from ARC. Generally, as shown in references, this is a method to treat data from ARC [31].

4. Simulation results

4.1. External temperature and cooling area effect on thermal-runaway

Using thermal-runaway model developed, thermal exposure test is simulated for 3.2 Ah prismatic cell of which cathode and anode consists of LCO and graphite, respectively. The simulation undergoes such condition that the external temperature increases from 130 [°C] to 170 [°C] by 10 [°C]. The outcome is plotted in Fig. 7. Through the simulation applying consistent temperature increment (10 [°C/min]) and maintenance time (1 h), it could be estimated that thermal-runaway do not occur when the ambient temperature changes in between 130 [°C] and 150 [°C], whereas it occurs in case the temperature rises over 160 [°C]. The simulation confirms qualitative result consistent with that of Kim et al., in which the verification of simulation is not justified through comparing it with experimental result yet [26]. For these reasons, thermal exposure test is carried out using a same cell which is subjected to the simulation, increasing the ambient temperature from 130 [°C] to 170 [°C] by 10 [°C]. As shown in Fig. 8, thermal-runaway do not occur when the ambient temperature changes in between 130 [°C] and 150 [°C] whereas it occurs in case the temperature rises over 160 [°C] in the experiment, which quantitatively matches with the simulation result. Thus the simulation model is verified, ready to be applied in another simulation. Considering the effect of electrolyte, the same formula of SEI decomposition was applied to thermal runaway model in Fig. 7. And also the values of activation energy and frequency factor from reference were used [26]. In general, the reaction of electrolyte is proceeded after thermal runaway has occurred. The same results were confirmed through our simulation research. Therefore, reaction of electrolyte was left out when the thermal runaway is simulated with other conditions. In Table 10, a virtual 3.2 Ah prismatic cell of the same volume used in verification case with different convective heat transfer area subjected to form-factor are listed. Thermal-runaway simulation is performed using these cells and the result is plotted in Fig. 9. Through the simulation, it is confirmed that thermal-runaway is delayed when the convective heat transfer area is augmented if the capacity and volume of the cell remains unchanged. Particularly, thermal-runaway does not occur when the ratio of convective heat transfer area to volume exceeds 2. Based on the result, it is manifested that the convective heat transfer area must increase if the capacity remains unchanged, lest thermal-runaway bust in. To execute the above simulation, convective heat transfer condition is set as boundary condition. Similar to the reference, when the temperature is increased in the simulation, the heat transfer coefficient is forced as 10 times of natural convective heat transfer coefficient 7.17 [W m^{-2} K^{-1}], which is 71.7 [W m^{-2} K^{-1}] to compensate for the effect of the fan in the chamber, but recovered to 7.17 [W m^{-2} K^{-1}] in maintenance section [28].

4.2. Reaction heat effect on thermal-runaway

Among the design variables, the effect of the loading level of active materials on thermal-runaway is speculated through the simulation in this chapter. In Fig. 10, the results of thermal-runaway simulation are comparing the effect of loading level under different electrical short circuit resistance. Heat generation is triggered by joule heating in short circuit region and internal resistive heating in jelly roll. The simulation treated two different cells using the same active material, of which loading level of each cathode are set as 44.9 [mg cm^{-2}] and 47.1 [mg cm^{-2}], and each anode are set as 21.8 [mg cm^{-2}] and 22.9 [mg cm^{-2}], respectively. 3 different cases of electrical short circuit resistance are simulated, 0.06 [Ω], 0.075 [Ω] and 0.08 [Ω]. As illustrated in Fig. 10, the possibility of thermal-runaway increases as the electrical short resistance decreases in both cases. As widely known, this result is attributed to upsurge in the electrical short circuit current by cause of small resistance, which, in turn, triggers heat generation of both joule heating by short circuit and internal resistance. However, it is also shown that thermal-runaway happens when the loading level of cathode is 47.1 [mg cm^{-2}], whereas it does not when loading level of cathode is decreased to 44.9 [mg cm^{-2}] under the same electrical short circuit resistance, 0.075 [Ω]. This is because more reactant participates in the reaction per a unit area if the loading level gets high, and thus the reaction rate rises. And the possibility for thermal-runaway is increased. In our study, a thermal runaway simulation is developed by using commercial LIBs which were in fresh condition. As generally known, there is no case for Li dendrite formation in fresh condition. Therefore, Li dendrite formation was not considered during short-circuit simulation. Besides, additional simulation is done to analyze the significance of DSC heat generation using two polymer cells of same loading level. The response is marked in Fig. 11. According to the result, thermal-runaway is more likely to occur if the electrical short circuit area extends regardless of kinds of active material, and this is because wide electrical short circuit area generates more resistive heat. There are mechanical safety tests for commercial LIBs such as impact or crush test. Therefore occurrence of thermal runaway can be confirmed by making the electrical short-circuit forcibly under mechanical safety test. Occurrence of the electrical short-circuit can confirm through changes of LIB voltage in safety test. However, area of short-circuit is generally unknown and it is hard to find through mechanical safety test. Thus, due to the area of electrical short-circuit that can't confirm, case study are processed that the height of electrical short was fixed as 1 [mm] and length was set as variable that determine short area. For this reason, the short area 0.5 [mm^2] is the assumption value for making the electrical short. When the same electrical short circuit area 2 [mm^2] is applied, however, thermal-runaway occurred in case the active material for cathode contains DSC heat generation of 619 [J/g], whereas DSC heat generation of 429 [J/g] is not sufficient for thermal-runaway. This is because the heat generation rate increases as chemical reaction is initiated by resistive heat generation, which is affected by the heat generation of active material, even though the loading level remains same. Therefore, when designing electrode, loading level must be low if the same material is used for electrode, or materials with low heat generation must be used for the same loading level, in order to obviate thermal-runaway by decreasing the rate of exothermic reaction.

4.3. Joule heat effect on thermal-runaway

So far, it has been speculated how a cell design variable influences thermal-runaway initiated by heat generation of electrical short circuit resistance through simulation. In Fig. 12, the influence of internal resistance of jelly roll on thermal-runaway is analyzed when the resistance caused by electrical short circuit remains identical, supplying the same heat generation to the cell. As shown in Fig. 12, it is confirmed that, were the electrical short circuit resistance not different, high internal resistance, i.e. 30 [mΩ] would trigger thermal-runaway, whereas low internal resistance, i.e. 25 [mΩ] would not. This is because high resistance causes more joule heat, hampering the safety of a cell. Thus, lowering the internal resistance of jelly roll prevents thermal-runaway when the other design variables are fixed. Next, it is also confirmed that the cell design variables have control over the heat generation of electrical short circuit resistance, although the value of short circuit resistance remains unchanged. Fig. 13 represents the relationship between the design variables and thermal-runaway caused by the resistive heat generation. Fig. 13 displays the simulation results regarding 2 different prismatic cells, comparing the effect of current density and thickness of electrode. The current density for each cell are set as 3.59 [mAh cm^{-2}] and 3.82 [mAh cm^{-2}], and the thickness of cathode electrode for each cell are set as 129 [μm] and 132 [μm]. In Fig. 13, thermal-runaway does not occur when high current density and thick electrode are applied, whereas thermal-runaway occurs in the opposite case. This is because the resistance of electrode increases along with the augmentation of current density and thickness of electrode, which weakens electrical short circuit current. Thus the resistive heat generation decreases and thermal-runaway hardly occurs. Consequently, it is advisable to increase the resistance resulted from the current density and the thickness of electrode when the same electrical short circuit condition is applied lest thermal-runaway occur.

5. Summary

In this paper, the thermal-runaway model is completed by combining resistive heating model with the electrochemical and exothermic reaction model of lithium-ion battery. Using the integrated model, the following conclusions are obtained regarding the simulation of thermal-runaway.

To prevent thermal-runaway.

- The convective heat transfer area should be increased if the capacity and volume of the cell are same.
- The loading level should be reduced if the electrical short circuit area is same.
- The heat generation of active materials should be decreased if the area of electrical short circuit area is same.
- The internal resistance of jelly roll should be decreased if the electrical short circuit current is same.
- The current density should be increased if the electrical short circuit resistance is same.

References

[1] P.G. Balakrishnan, R. Ramesh, T. Prem Kumar, J. Power Sources 155 (2006) 401–414.
[2] Y. Zeng, K. Wu, D. Wang, Z. Wang, L. Chen, J. Power Sources 160 (2006) 1302–1307.
[3] Y.-S. Chen, C.-C. Hub, Y.-Y. Li, J. Power Sources 181 (2008) 69–73.
[4] R.A. Leising, M.J. Palazzo, E.S. Takeuchi, K.J. Takeuchi, J. Electrochem. Soc. 148 (2001) A838–A844.
[5] P. Arora, M. Doyle, R.E. Whitea, J. Electrochem. Soc. 146 (1999) 3543–3553.
[6] T. Ohsaki, T. Kishi, T. Kuboki, N. Takami, N. Shimura, Y. Sato, M. Sekino, A. Satoh, J. Power Sources 146 (2005) 97–100.
[7] R. Spotnitz, J. Franklin, J. Power Sources 113 (2003) 81–100.
[8] H. Wu, D. Zhuo, D. Kong, Y. Cui, Nat. Commun. 5 (2014) 5193, http://dx.doi.org/10.1038/ncomms6193.
[9] T.F. Fuller, M. Doyle, J. Newman, J. Electrochem. Soc. 141 (1994) 1–10 echem model.
[10] J. Newman, J. Electrochem. Soc. 142 (1995) 97–101.
[11] J. Christensen, D. Cook, P. Albertus, J. Electrochem. Soc. 160 (2013)

A2258–A2267.
[12] T.-S. Dao, C.P. Vyasarayani, J. McPhee, J. Power Sources 198 (2012) 329–337.
[13] N. Nieto, L. uis Díaz, J. Gastelurrutia, I. Alava, F. Blanco, J.C. Ramos, A. Rivas, J. Electrochem. Soc. 160 (2013) A212–A217.
[14] M. Guo, G. Sikha, R.E. White, J. Electrochem. Soc. 158 (2011) A122–A132.
[15] D.H. Jeon, S.M. Baek, Energy Convers. Manag. 52 (2011) 2973–2981.
[16] X. Zhang, Electrochim. Acta 56 (2011) 1246–1255. Thermal Analysis.
[17] V.R. Subramanian, V.D. Diwakar, D. Tapriyal, J. Electrochem. Soc. 152 (2005) A2002–A2008.
[18] K. Smith, C.-Y. Wang, J. Power Sources 160 (2006) 662–673.
[19] V. Srinivasan, C.Y. Wang, J. Electrochem. Soc. 150 (2003) A98–A106.
[20] L. Song, J.W. Evans, J. Electrochem. Soc. 147 (2000) 2086–2095.
[21] S.A. Hallaj, H. Maleki, J.S. Hong, J.R. Selman, J. Power Sources 83 (1999) 1–8.
[22] M.N. Richard, J.R. Dahn, J. Electrochem. Soc. 146 (1999) 2068–2077.
[23] M.N. Richard, J.R. Dahn, J. Electrochem. Soc. 146 (1999) 2078–2084.
[24] D.D. MacNeil, L. Christensen, J. Landucci, J.M. Paulsen, J.R. Dahn, J. Electrochem. Soc. 147 (2000) 970–979.
[25] T.D. Hatchard, D.D. MacNeil, A. Basu, J.R. Dahn, J. Electrochem. Soc. 148 (2001) A755–A761.
[26] G.-H. Kim, A. Pesaran, R. Spotnitz, J. Power Sources 170 (2007) 476–489.
[27] S. Santhanagopalan, P. Ramadass, Z. Zhang, J. Power Sources 194 (2009) 550–557.
[28] K.-C. Chiu, C.-H. Lin, S.-F. Yeh, Y.-H. Lin, K.-C. Chen, J. Power Sources 251 (2014) 254–263.
[29] N. Nieto, L. Díaz, J. Gastelurrutia, F. Blanco, J.C. Ramos, A. Rivas, J. Power Sources 272 (2014).
[30] Q. Wang, P. Ping, X. Zhao, G. Chu, J. Sun, C. Chen, J. Power Sources 208 (2012) 210–224.
[31] X. Feng, M. Fang, X. He, M. Ouyang, L. Lu, H. Wang, M. Zhang, J. Power Sources 255 (2014) 294–301.

Nomenclature

a: specific interfacial area, $m^2\ m^{-3}$
A: frequency factor, s^{-1}
C: concentration of salt in electrolyte, mol m^{-3}
C_s: concentration of lithium in electrode, mol m^{-3}
C_p: heat capacity, J $kg^{-1}\ K^{-1}$
D: electrolyte phase lithium-ion diffusivity, $m^2\ s^{-1}$
D_s: solid phase lithium diffusivity, $m^2\ s^{-1}$
E: activation energy, eV
F: Faraday constant, 96485C mol^{-1}
h: specific energy, J g^{-1}
I: total current density, A m^{-2}
i_1: solid phase current density, A m^{-2}
i_2: electrolyte phase current density, A m^{-2}
j_n: pore wall flux of lithium-ion, mol $m^{-2}\ s^{-1}$
k_B: Boltzmann's constant, eV K^{-1}
Q: heat generation rate, W m^{-3}
R: gas constant, 8.314 J K^{-1} mol^{-1}
$R_{external\ short}$: short-circuit resistance, Ω
R_s: radius of electrode particle, um
T: temperature, K
t: time, s
t^+: transference number
U_k: open-circuit potential at 25 °C, V
u: degree of conversion
x_i: amount of intercalated lithium
x_f: amount of meta-stable SEI
z: amount of lithium in the SEI per unit surface area, m^2
z_o: initial amount of lithium in the SEI per unit surface area, m^2
α: symmetric factor
β: parameter of autocatalysis
ε: porosity of electrode
ϕ_1: electric potential of solid phase, V
ϕ_2: electric potential of electrolyte phase, V
η_s: surface over-potential, V
κ: liquid phase conductivity, S m^{-1}
λ: thermal conductivity, W $m^{-1}\ K^{-1}$
ρ: density, kg m^{-3}
σ: solid phase electric conductivity, S m^{-1}

Subscript

eff: effective
ohm: ohmic heat generation
rev: reversible heat generation
rxn: reaction heat generation